IDEAL MHD STABILITY OF INTERNAL KINKS IN CIRCULAR AND SHAPED TOKAMAKS

H. LÜTJENS, A. BONDESON
Centre de recherches en physique des plasmas,
Association Euratom-Confédération Suisse,
Ecole polytechnique fédérale de Lausanne,
Lausanne, Switzerland

G. VLAD
Centro Ricerche Energia Frascati,
Associazione Euratom-ENEA sulla Fusione,
Frascati, Rome, Italy

ABSTRACT. Stability limits for the internal kink mode are calculated for tokamaks with different current profiles and plasma cross-sections using ideal magnetohydrodynamics (MHD). The maximum stable poloidal beta at the q = 1 surface (β_p) is sensitive to the current profile, but for circular cross-sections it is typically between 0.1 and 0.2. Large aspect ratio theory gives similar predictions when the appropriate boundary conditions are applied at the plasma-vacuum surface. It is found that the internal kink is significantly destabilized by ellipticity. For JET geometry, the ideal MHD limit in β_p is typically between 0.03 and 0.1, and arbitrarily low limits can result if the shear is reduced at the q = 1 surface. A large aspect ratio expansion of the Mercier criterion retaining the effects of ellipticity and triangularity is used to illustrate the destabilizing influence of ellipticity.

1. INTRODUCTION

Ideal MHD theory has been successful in predicting the global operational limits for tokamaks. However, for sawtooth oscillations, triggered by internal kinks of toroidal mode number n = 1, the theoretical understanding is at present very incomplete. The uncertainties are manyfold. It is not well understood what is the appropriate physics model, and experimental information on the plasma profiles is scarce and uncertain, in particular for the current distribution. Another uncertainty comes from poor understanding of the stability limits even in the simplest theoretical model — ideal MHD. In this paper, we present a numerical and analytical study to clarify the ideal MHD stability of the internal kink. We find that the pressure limit is significantly lower than previously assumed, in particular for elliptically shaped cross-sections.

Bussac et al. [1] calculated the pressure limit for internal kink stability in circular equilibria by a large aspect ratio expansion. For a parabolic current profile and a small q = 1 radius, they found that the mode is stable when $\beta_p < (13/144)^{1/2} \approx 0.3$. In carrying out numerical calculations at finite aspect ratio, we generally found significantly lower pressure limits. We will show that the main reason for this difference is not the finite aspect ratio but rather the choice of boundary conditions. The results of Ref. [1] for the parabolic current profile are strongly influenced by the assumption of a rigid wall at the edge of the plasma, r = a, when the safety factor at the edge, q_a, is below 2. Tokamaks are normally operated with $q_a > 2$. Here, we consider the large aspect ratio theory for circular tokamaks with a modified treatment of the boundary. Thus, for current profiles such that $q_a < 2$, we replace the conducting wall at r = a [1] by a perfectly conducting, currentless plasma that extends beyond the q = 2 surface. With this prescription, the large aspect ratio expansion gives β_p limits that are typically between 0.1 and 0.2 for rounded current profiles, in good agreement with the numerical results at finite aspect ratio. (We note that rather low β_p limits, in the range of 0 and 0.1, have been found previously from the large aspect ratio expansion for special current profiles [2, 3] using boundary conditions appropriate for $q_a > 2$). With the appropriate boundary conditions, the β_p limit predicted by the large aspect ratio expansion decreases with increasing q = 1 radius and, for q_0 below some profile dependent threshold, the n = 1 internal kink is unstable at zero beta, also in accordance with numerical results at finite aspect ratio [4].

With respect to shaping, analytical studies [3, 5] suggest that the effect of ellipticity is weak when the

central safety factor q_0 is close to unity, whereas numerical computations show clear destabilization by elliptic shaping [6–8]. Our numerical calculations, without recourse to geometrical orderings, confirm that ellipticity is strongly destabilizing, in particular for low central shear. The main part of this destabilization results from ellipticity in combination with finite pressure and finite aspect ratio. Terms of this order have hitherto been disregarded in analytical large aspect ratio expansions [3, 5]. As an analytical example of this destabilization, we present the large aspect ratio expression for the Mercier criterion which includes the effects of ellipticity and triangularity.

In a recent numerical study [7], Coppi and Coppi also concluded that the ideal MHD beta limit for the internal kink mode is lower than previous analytic studies indicate. (Unfortunately, the pressure limit in Ref. [7] is quoted in terms of the poloidal beta at the edge, making it somewhat difficult to compare these thresholds with those of analytic theory or of the present paper, where the limit is given in terms of poloidal beta at the q = 1 surface.) Possible consequences of the low beta limits for the internal kink for the design and operation of the next generation of tokamaks are discussed in Ref. [7]. The lower ideal MHD thresholds found here and in Ref. [7] may also affect the theoretical interpretation of existing experimental data.

2. EFFECTS OF CIRCULAR CROSS-SECTION AND CURRENT PROFILE

2.1. Large aspect ratio expansion

Stability limits for the internal kink mode have been calculated by means of the large aspect ratio expansion [1], taking into account the toroidal coupling of the dominant m = 1 displacement (m is the poloidal mode number) to the m = 0 and m = 2 side-bands. For a parabolic current profile, Bussac et al. [1] found that the marginally stable value of β_p is about 0.3 when $r_{q=1} \ll a$, falls to a minimum of about 0.23 when $r_{q=1}/a \approx 0.4$, and then increases again for larger q = 1 radii. For profiles that are more peaked than parabolic, the pressure limit decreases more sharply with $r_{q=1}$. Very steep current profiles, such as the Shafranov (step function) profile, are less stable [3].

The stability diagram ($\beta_{p,crit}$ versus $r_{q=1}/a$) of Bussac et al. [1] was computed assuming a fixed plasma boundary. With this assumption, the m = 2 side-band is wall stabilized whenever $q_a < 2$. For the parabolic current profile, $q_a/q_0 = 2$, and therefore $q_a < 2$ holds if $q_0 < 1$, i.e. in all cases of interest for the internal kink. Evidently, the results in Ref. [1] for the parabolic profile refer to the non-standard case of very low q operation, $q_a < 2$, with a close fitting wall. Although tokamaks can be operated in this way, the standard operating regime is $q_a > 2$. In all calculations presented in this paper, $q_a > 2$ is assumed.

For comparison with the finite aspect ratio computations, we have recomputed the β_p limit using the large aspect ratio theory and boundary conditions appropriate for $q_a > 2$. Figure 1 shows the results for different current profiles: two polynomial profiles

$$j(r) = \begin{cases} j_0(1 - r^2/a^2)^\ell & r < a \\ 0 & r > a \end{cases} \quad (1)$$

with $\ell = 1, 2$ (parabolic and parabolic squared) for which $q_a = (\ell+1)q_0$, and the Shafranov profile, with the step in the current density at $r = r_0 = 0.5a$.

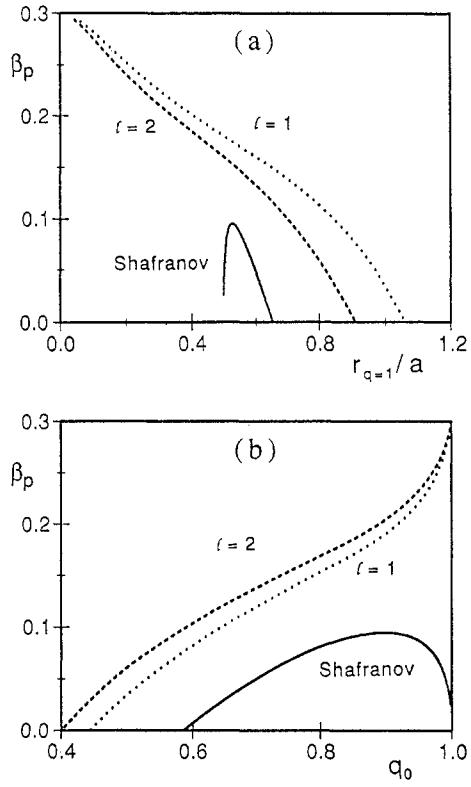

FIG. 1. Marginal β_p for circular equilibria from large aspect ratio theory. Results are given for three current profiles: Shafranov (with the step at $r_0 = a/2$), parabolic ($\ell = 1$) and parabolic squared ($\ell = 2$), in (a) versus $r_{q=1}/a$ and in (b) versus q_0.

We assume that the q = 2 surface lies within the conducting plasma, and if $q_a < 2$, we add a region of currentless but perfectly conducting plasma that extends to the q = 2 surface at $r/a = (2/q_a)^{1/2}$. (In this case, 'a' denotes the radius of the current channel, not the plasma radius.) For the two smooth profiles (1), the β_p limit falls monotonically when the q = 1 radius increases, as shown in Fig. 1(a). This is in clear contrast to the result of Ref. [1] for the parabolic profile, where the stabilization by the wall at r = a becomes stronger with increasing q = 1 radius and the pressure limit even goes to infinity for $r_{q=1}/a > 0.79$. With the modified treatment of the wall, we find 'typical' limits in the range of 0.1 to 0.2 rather than the usually quoted value 0.3, which is valid as $r_{q=1}/a \to 0$.

Figure 1 shows that the β_p limit goes to zero for q_0 below some profile dependent threshold, ranging from 0.40 for the parabolic squared profile to 0.58 for the Shafranov profile. For q_0 close to unity, the pressure limit is highly sensitive to the current profile; the Shafranov profile gives much lower values than the rounded off current profiles (1).

2.2. Finite aspect ratio calculations and definitions

We have numerically calculated the full MHD stability limits for the internal kink at finite aspect ratio using the stability code MARS [8] and the equilibrium code CHEASE [9]. The plasma vacuum surface in equilibrium is prescribed as

$$R = R_0 + a\cos(\theta + \delta\sin\theta)$$
$$Z = a\kappa\sin\theta \qquad (2)$$

where κ is the elongation and δ is the triangularity. Results will be presented for two geometries, corresponding to the TEXTOR tokamak with $R_0/a = 4$, $\kappa = 1$, $\delta = 0$ (medium aspect ratio circle), and to JET with $R_0/a = 2.7$, $\kappa = 1.7$, $\delta = 0.3$ (small aspect ratio dee).

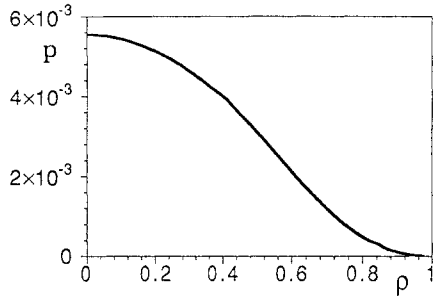

FIG. 2. Pressure versus normalized minor radius ρ for the numerical equilibria.

In all cases, we have used the same pressure profile p/p_0. The pressure is prescribed as a function of the poloidal flux ψ, such that $dp/d\psi$ is constant in the central region and falls to zero smoothly at the edge. Figure 2 shows the pressure versus the normalized minor radius $\rho \equiv [V(\psi)/V_{tot}]^{1/2}$, where $V(\psi)$ is the volume enclosed by a constant-ψ surface.

The current profiles are specified by the surface averaged toroidal current density

$$I^* \equiv \frac{\int j_\phi (J/R)\,d\chi}{\int (J/R)\,d\chi} \qquad (3)$$

(where J is the Jacobian for the transformation from flux co-ordinates (ψ, χ, ϕ) to Cartesian co-ordinates) as a function of the normalized poloidal flux ψ/ψ_{axis}. $I^*(\psi/\psi_{axis})$ is prescribed, except for a multiplicative factor that is adjusted to specify the q = 1 radius.

Two important quantities characterizing the equilibria are the shear

$$s \equiv \frac{\rho}{q}\frac{dq}{d\rho} \qquad (4)$$

and the poloidal beta

$$\beta_p(\psi) \equiv -\frac{4}{\mu_0 I_\phi^2(\psi) R_0}\int_0^\psi \frac{dp}{d\psi'} V(\psi')\,d\psi' \qquad (5)$$

where $I_\phi(\psi)$ is the toroidal current within a constant-ψ surface. The poloidal beta at the q = 1 surface is denoted β_p.

The stability diagrams presented in the following give β_p as a function of the q = 1 radius $\rho_{q=1}$ at constant growth rates, $\gamma/\omega_A = 0$, 1×10^{-3}, 3×10^{-3} and 5×10^{-3}, where $\omega_A = v_A/R_0$ is the toroidal Alfvén frequency. These curves have been obtained after interpolation of the computed values of $\gamma(\beta_p, \rho_{q=1})$ for equilibria with different β_p but identical I^* profiles.

We have carried out convergence studies and the results are shown after extrapolation to zero mesh size; however, it must be admitted that ideal MHD growth rates of the order of $10^{-3}\,\omega_A$ are non-trivial to compute. Our results for $\gamma = 10^{-3}\,\omega_A$ should be reliable, but, in certain cases, extrapolation to marginal stability is somewhat uncertain. This may be acceptable from a physics point of view, since instabilities with very small growth rates must be expected to be strongly modified by non-MHD effects.

2.3. Numerical results for a circular boundary

We have studied four different current profiles for plasmas with a circular boundary and a fixed aspect ratio of 4: one *rounded* profile, two profiles with I^*

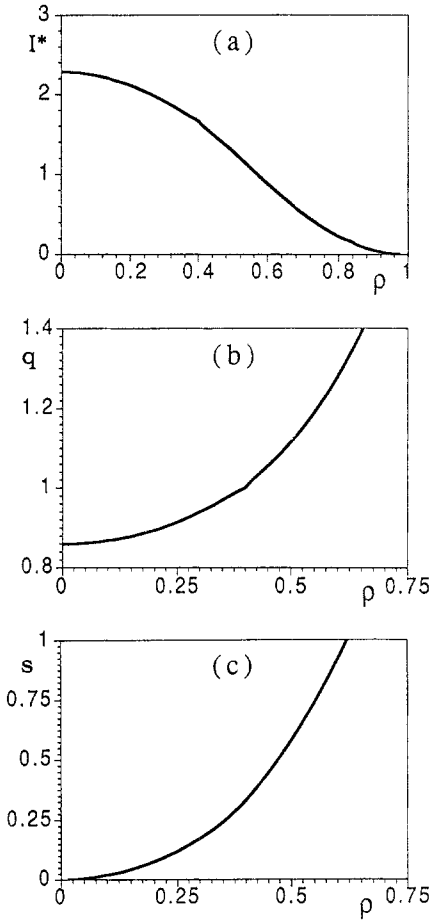

FIG. 3. Profiles of (a) averaged toroidal current density I^*, (b) safety factor q and (c) shear s versus ρ for the rounded current profile.

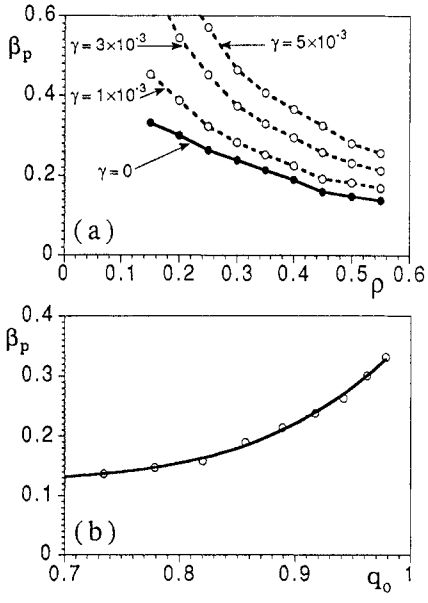

FIG. 4. Stability limits in β_p for circular equilibrium with aspect ratio 4 and the rounded current profile shown in Fig. 3. (a) β_p versus $\rho_{q=1}$ and (b) β_p versus q_0.

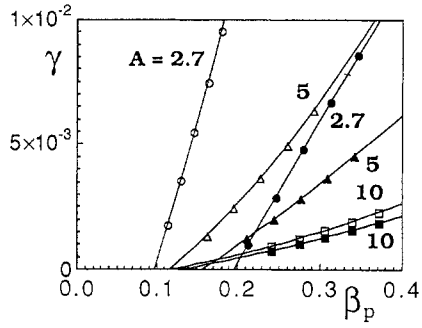

FIG. 5. Internal kink growth rates versus β_p for a circular equilibrium with fixed boundary (filled symbols) and free boundary (open symbols). Three different aspect ratios are shown: $A = R_0/a = 10$, 5 and 2.7, and $\rho_{q=1} = 0.6$.

flattened at a certain radius, and a profile where I^* has 'shoulders', termed TEXTOR [10].

Figure 3 shows $I^*(\rho)$, $q(\rho)$ and $s(\rho)$ for the *rounded* profile, and Fig. 4 shows the corresponding stability results. Both the current profile and the marginal stability curve are close to those for the parabolic squared profile of Section 2.1. Figure 4(b) shows the marginal β_p versus q_0, to be compared with Fig. 1(b). Evidently, for an aspect ratio of 4 and a circular boundary the large aspect ratio theory is in good agreement with the full-MHD result.

Figure 5 shows an effect that is a higher order correction to the large aspect ratio result: the influence of the wall position for circular equilibria with $2 < q_a < 3$. The diagram shows the growth rates of the n = 1 internal kink for different aspect ratios and a circular boundary, with the boundary either fixed or free (and the wall at infinity). For circular equilibria with $q_a > 2$, the large aspect ratio expansion to lowest order shows no effect of the wall position. According to Fig. 5, this is a good approximation at large aspect ratio, A = 10. A detailed analysis of the numerical results shows that the difference in marginal β_p between the free and fixed boundary cases is proportional to $(a/R_0)^2$ at large aspect ratio. At tight aspect ratio, A = 2.7, the difference between the fixed and free boundary results is appreciable: $\beta_p \approx 0.1$ for a free boundary and $\beta_p \approx 0.2$ for a fixed boundary. The numerical results show a very weak influence of the wall position for circular equilibria with $q_a > 3$.

We conclude that the wall position influences the internal kink stability for aspect ratios of interest only at low q_a. In the following, we consider configurations where the wall is placed 20% of the minor radius away from the plasma.

The *flattened* current profiles (Fig. 6) have a plateau at a certain radius: $dI^*/d\rho = 0$ for $\rho = \rho_p \sim 0.42$. Inside this radius the shear is rather uniform and on the outside it increases sharply. We consider two profiles with different central shear: one with small central shear, $q_0/q(\rho_p) \approx 0.95$, and one with medium central shear, $q_0/q(\rho_p) \approx 0.80$.

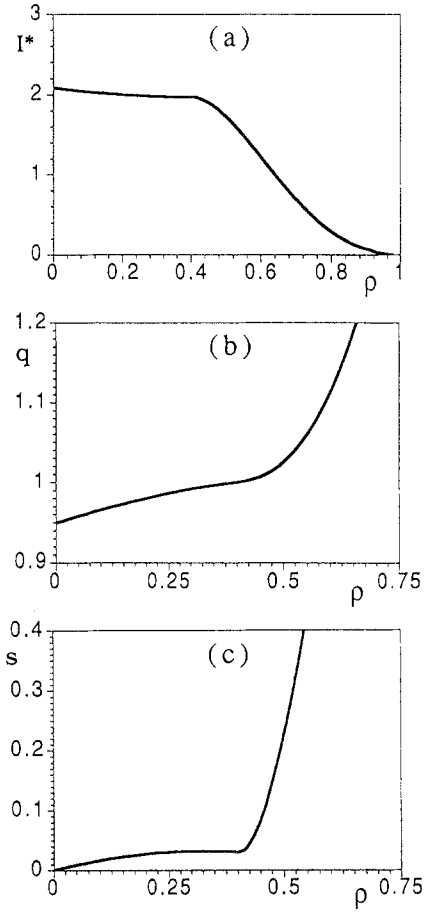

FIG. 6. Profiles of (a) averaged toroidal current density I^*, (b) safety factor q and (c) shear s versus ρ for the flattened current profile with low central shear.

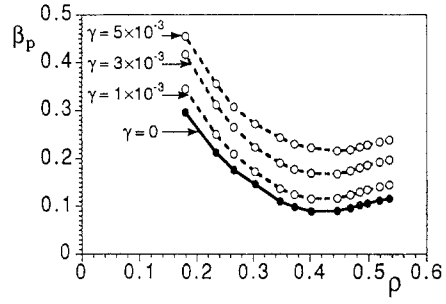

FIG. 7. Stability limits in β_p for the flattened current profile with low central shear (Fig. 6). The cross-section is circular with A = 4.

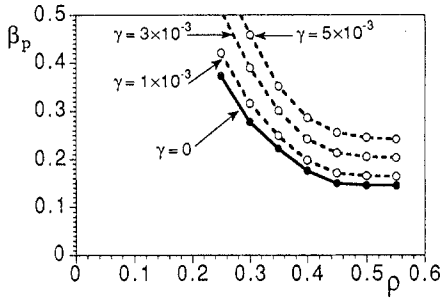

FIG. 8. Stability limits in β_p for the flattened current profile with higher central shear (four times larger than in Fig. 6). The cross-section is circular with A = 4.

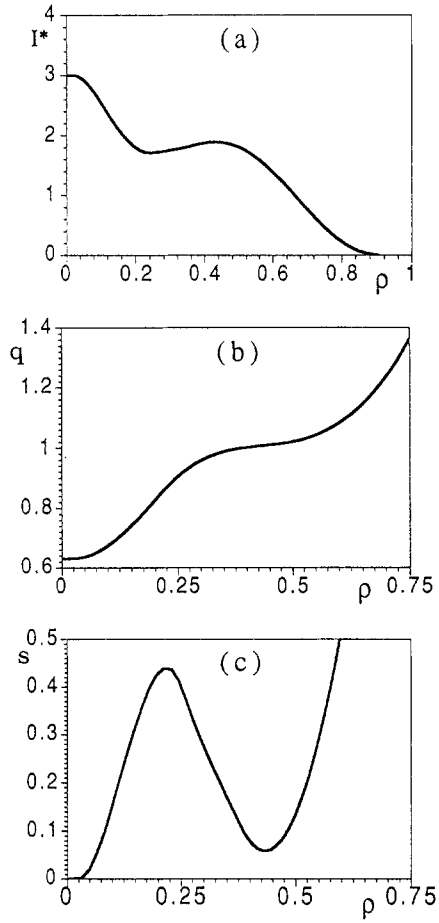

FIG. 9. Profiles of (a) averaged toroidal current density I^*, (b) safety factor q and (c) shear s versus ρ for the TEXTOR profile.

Figure 6 shows $I^*(\rho)$, $q(\rho)$ and $s(\rho)$ for the flattened profile with low central shear at aspect ratio 4, and Fig. 7 shows the stability results. The marginal β_p is similar to that for the rounded profile (Fig. 4) when the q = 1 surface is far away from the current plateau at $\rho \sim 0.42$, but when the q = 1 surface is near the plateau, $\beta_{p,crit}$ has a local minimum of about 0.08.

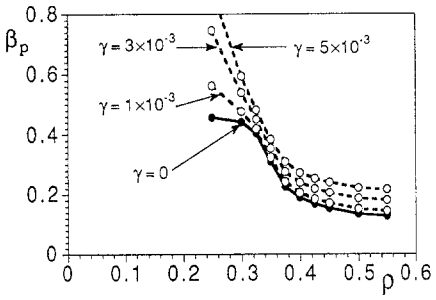

FIG. 10. Stability limits in β_p for the TEXTOR current profile in Fig. 9. The cross-section is circular with A = 4.

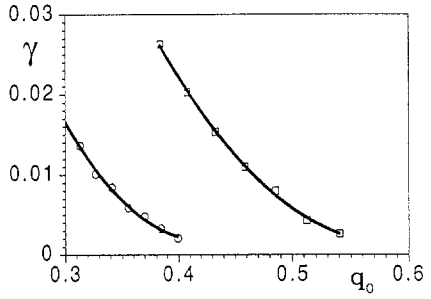

FIG. 11. Internal kink instability at zero pressure for a low q_0, circular equilibrium (A = 4) with the rounded current profile (circles) and the Shafranov profile (squares).

Figure 8 shows the stability limits for the flattened current profile with medium central shear. The equilibrium is similar to that in Fig. 6, except that the central shear is four times larger. The limits in β_p are higher than those for the low shear equilibrium. They are quite similar to those for the rounded profile (Figs 3, 4), except for slightly higher values when the q = 1 radius is small owing to the higher shear near the magnetic axis.

Finally, Figs 9 and 10 give profiles and stability limits for a current profile of the TEXTOR type with shoulders at $\rho \sim 0.4$. The marginal β_p has a rather high maximum (≈ 0.46) when the q = 1 surface is located slightly inside the shoulders, but $\beta_{p,crit}$ falls abruptly to between 0.1 and 0.2 when the q = 1 radius increases and reaches the low shear region. The TEXTOR profile is particularly stable to the internal kink mode and can even be resistively stable at fairly high β_p [8, 10, 11].

The large aspect ratio results (Section 2.1) show that the n = 1 mode is unstable even at zero pressure when q_0 is below a threshold value ranging from 0.58 for the Shafranov profile to 0.40 for the parabolic squared profile. We have studied this current driven mode for two finite aspect ratio equilibria with zero pressure: (a) the rounded profile and (b) the Shafranov profile, both surrounded by a region of currentless but conducting plasma. The aspect ratios (R_0/a for the rounded profile and R_0/r_0 for the Shafranov profile, where r_0 is the radius of the step) are 4 in both cases. Figure 11 shows the resulting growth rates as functions of q_0. Instability occurs below certain thresholds in q_0, which are in remarkably good agreement with the large aspect ratio result (Fig. 1). The instability at low q_0 has been observed previously by Turnbull and Troyon [4]. It is sensitive to the current profile, and the Shafranov profile is more unstable than the rounded profiles.

The results for circular equilibria can be simply summarized. Except at very low aspect ratio, the stability of the internal kink is in good agreement with the large aspect ratio theory when the appropriate boundary conditions are applied. For smooth and monotonic current profiles, the marginal β_p decreases monotonically with increasing q = 1 radius, and the typical β_p limits are between 0.1 and 0.2. The position of the wall is important only for tight aspect ratio and $q_a < 3$.

3. SHAPING EFFECTS

3.1. Numerical results for JET geometry

It is well known that internal kinks are destabilized by ellipticity [6, 12]. To illustrate this, we give numerical results for the full ideal MHD stability problem in JET geometry: aspect ratio A = 2.7, elongation $\kappa = 1.7$ and triangularity $\delta = 0.3$ for the same current profiles as those for the circular cross-section. The $q(\rho)$ and $s(\rho)$ profiles are slightly different from their circular equivalents, but the differences are insignificant in the central region, say $\rho < 0.6$.

The β_p limits for the JET geometry are significantly lower than those for the circle. The results for the rounded current profile are shown in Fig. 12. The maximum stable β_p is about 0.09 and the limit decreases as the q = 1 surface approaches the magnetic axis. The effect of ellipticity was estimated analytically in Refs [3, 5] by computing the shaping contribution to δW at infinite aspect ratio and zero pressure. This shaping term was found to have a vanishing effect on the marginal β_p as $q_0 \rightarrow 1$. By contrast, the full MHD result in Fig. 12 shows that the β_p limit is strongly reduced for the JET shape and small q = 1 radius. In fact, with the JET shape, $\beta_{p,crit}$ vanishes, or is very small, as $q_0 \rightarrow 1$.

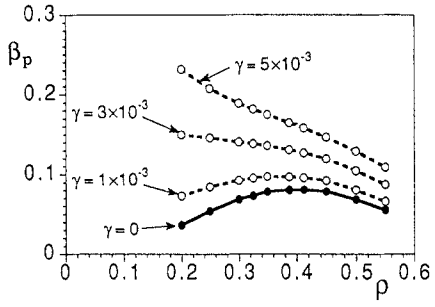

FIG. 12. Stability limits in β_p for JET geometry and the rounded current profile (Fig. 3).

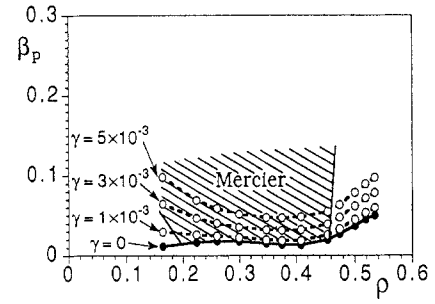

FIG. 13. Stability limits in β_p for JET geometry and the flattened current profile with low central shear (Fig. 6). The hatched region indicates violation of the Mercier criterion at q = 1.

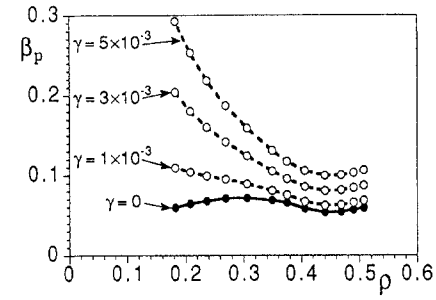

FIG. 14. Stability limits in β_p for JET geometry and the flattened current profile with higher central shear.

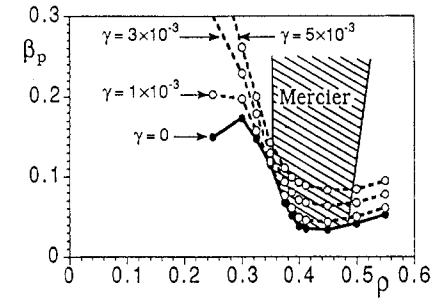

FIG. 15. Stability limits in β_p for JET geometry and the TEXTOR current profile (Fig. 9). The hatched region indicates violation of the Mercier criterion at q = 1.

Similarly, for the two flattened current profiles, the beta limits are lower for the JET cross-section than for a circle, see Figs 13 and 14. The decrease is rather dramatic for the profile with weak central shear, for which the β_p limit in JET geometry is typically around 0.03, while for the medium shear profile it is about 0.08. Thus, contrary to the predictions of earlier analytical expansions [3, 5], the destabilization is stronger in the case of weak central shear. This destabilization by shaping can be correlated with interchange instability. The hatched region of Fig. 13 shows where the Mercier criterion is violated on the q = 1 surface. The minimum in $\beta_{p,crit}$ is set by interchange instability for this equilibrium. It is well known [13] that, when the Mercier criterion is violated on a rational surface q = m/n, there exist (infinitely many) unstable modes with toroidal mode number n. Our numerical calculations show that violation of the Mercier criterion on the q = 1 surface leads to an n = 1 internal mode, typically with a large growth rate.

Further evidence of the importance of interchange stability can be found in the stability diagram for the TEXTOR current profile, Fig. 15. This figure shows a clear dependence on the shear locally at the q = 1 surface. The β_p limit drops from about 0.17 (the highest value we have found with JET geometry) when the q = 1 surface is in the high shear region inside the shoulders, to about 0.03 when the q = 1 surface enters the region of minimum shear. The minimum in $\beta_{p,crit}$ again coincides with the threshold for interchange at the q = 1 surface and increases if the minimum shear is increased. Figure 16 shows the stability diagram for a TEXTOR profile with reduced shoulders and larger minimum shear ($s_{min} = s(\rho \approx 0.38) \approx 0.16$). Note the absence of a local minimum in the marginal β_p at the radius of minimum shear for this equilibrium.

It is of interest to consider the shape of the unstable eigenfunction when the Mercier criterion is violated at the q = 1 surface. This reveals that, when the Mercier criterion is violated only in a small region around the q = 1 surface, the mode structure is quite different from the usual step function. As an example, Fig. 17(a) shows the unstable displacement for the JET cross-section and the TEXTOR current profile, with the q = 1 surface at the point of minimum shear, at two different pressures. In the lowest beta case, the Mercier criterion is violated only in a small region around q = 1 and the unstable mode has a clear interchange character. However, for a relatively moderate β_p, the mode resembles the standard step function of the internal kink. In cases where the Mercier criterion is violated more globally in the q < 1 region, the

unstable mode stays close to the step function also near the marginal point, as shown in Fig. 17(b) for the low shear profile. (It should be noted that the eigenfunction can lose its structural stability as marginal stability is approached.)

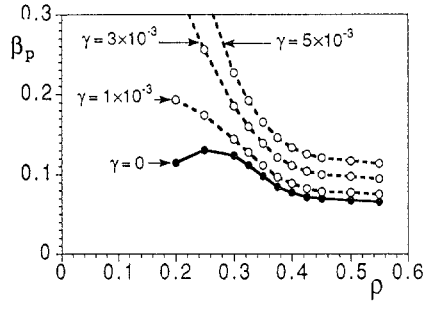

FIG. 16. Stability limits in β_p for equilibria with JET geometry and the TEXTOR current profile with reduced shoulders.

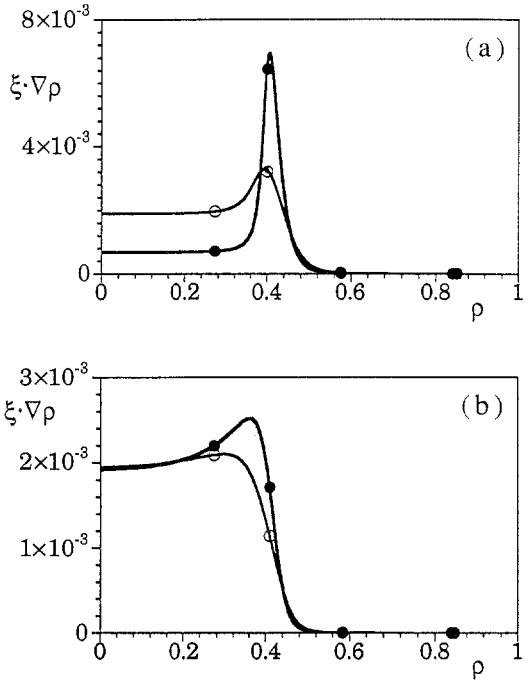

FIG. 17. Eigenfunctions (m = 1 components of $\xi\cdot\nabla\rho$ in straight field line co-ordinates) for different cases with the JET cross-section when the Mercier criterion is violated at the q = 1 surface. (a) The TEXTOR current profile (Fig. 15) with $\rho_{q=1} = 0.4$ and the Mercier criterion is violated only locally. The two cases have $\beta_p = 0.043$, $\gamma = 9.9 \times 10^{-4}$ (filled circles) and $\beta_p = 0.096$, $\gamma = 4.2 \times 10^{-3}$ (open circles). (b) The low shear current profile (Figs 6 and 13) with $\rho_{q=1} \sim 0.41$. The Mercier criterion is violated globally for $q < 1$. The two cases have $\beta_p = 0.025$, $\gamma = 2.0 \times 10^{-3}$ (filled circles) and $\beta_p = 0.042$, $\gamma = 4.1 \times 10^{-3}$ (open circles).

The numerical results of this section show that the ideal MHD pressure limit for the internal kink is significantly lower for JET geometry than for a circle. For most of the JET cases we have examined, the critical β_p is below 0.1. With elliptic shaping and weak shear, the Mercier criterion can be violated at low β_p, and this generally gives rise to global instabilities with large growth rates.

3.2. Large aspect ratio Mercier criterion including shape effects

Comparison of the results for the circular and the JET shaped cross-sections shows that ellipticity is destabilizing. The destabilization is particularly noticeable at low shear, contrary to the large aspect ratio prediction of Refs [3, 5]. However, the shape corrections in Refs [3, 5] were evaluated at infinite aspect ratio and zero pressure, while the destabilization of the internal kink in our numerical examples with low shear is connected with violation of the Mercier criterion on q = 1. This instability is well known; for vertically elongated flux surfaces, the Mercier criterion on the magnetic axis [14] is violated when q = 1 (unless the triangularity is sufficiently large). It is evident that terms which are normally 'small' in the large aspect ratio expansion can become non-negligible for equilibria with weak shear.

It would be desirable to express the ellipticity corrections to the potential energy of the internal kink by extending the large aspect ratio calculation of Bussac et al. [1]. This entails retaining the toroidicity and ellipticity induced couplings of the m = 1 component to its four side-bands, m = −1, 0, 2, 3, and calculating all $O(\epsilon^2 e)$ terms (where $\epsilon = r_{q=1}/R_0$ and e is the ellipticity) in $\delta W/\epsilon^2$. This is a rather formidable calculation, and, to illustrate the point, we shall content ourselves by giving the corrections to the Mercier criterion due to ellipticity and triangularity at large aspect ratio.

We modify the standard large aspect ratio expansion by introducing two small parameters: toroidicity, $\epsilon(=r/R_0)$, and ellipticity, $e(=(\kappa-1)/2)$. The poloidal beta and the safety factor q will be considered to have order one. The expansion will be taken to second order in ϵ and to first order in e, *keeping* the contributions of order $\epsilon^2 e$. This is justified because the normally leading $O(\epsilon^2)$ pressure contribution to the Mercier parameter vanishes for q = 1, so that the $O(\epsilon^2 e)$ shaping terms give the leading contribution. We stress the importance of ordering ellipticity independently from aspect ratio. Connor and Hastie [5] set

$e = O(\epsilon)$ which makes the ellipticity induced terms higher order in ϵ (and, in the limit of infinite aspect ratio, the equilibrium is circular). The modified ordering allows us to calculate the contribution due to elliptic and triangular shaping without going beyond second order in ϵ.[1] Except for the difference in ordering, our calculation follows that of Connor and Hastie [5]. The flux surfaces are assumed to have the shape

$$R = R_0 - \epsilon[r - eE(r)]\cos\omega - \Delta(r) + \epsilon^2 T(r)\cos 2\omega + \epsilon^3 P\cos\omega + \ldots$$
$$Z = \epsilon[r + eE(r)]\sin\omega + \epsilon^2 T(r)\sin 2\omega - \epsilon^3 P\sin\omega + \ldots \quad (6)$$

where r and ω are two non-orthogonal co-ordinates corresponding to minor radius and poloidal angle, and ϵ and e are independent expansion parameters. The elliptic deformation E(r) is related to the elongation by $\kappa = 1 + 2E/r + O((E/r)^2)$, $\Delta(r)$ is the Shafranov shift and T(r) is the triangular deformation related to the triangularity by $\delta = 4T(r)/r$. Using the double expansion, we obtain in the Appendix the Mercier criterion, to second order in ϵ and first order in e, as

$$-D_I = \frac{1}{4} + \frac{2p'}{rB^2}\frac{q^2}{q'^2}\left[1 - q^2 + \frac{3q^2}{4} \times \left(\frac{E}{r} + E'\right) + \frac{3q^2}{2}\Lambda\left(\frac{E}{r} - E'\right) - \frac{R_0 q^2}{r}\left(\frac{2ET}{r^2} + \frac{6E'T}{r} + \frac{7ET'}{2r} - \frac{3}{2}E'T'\right)\right] > 0 \quad (7)$$

Here, the prime denotes differentiation with respect to the minor radius r, and $\Lambda \equiv R_0\Delta'/r \approx \beta_p(r) + \ell_i(r)/2$, where $\ell_i(r)$ is the internal inductance. Equation (7) generalizes the formula for the circular flux surfaces of Shafranov and Yurchenko [16] and Glasser et al. [17] and is consistent with previous expressions retaining shaping effects near the magnetic axis [14]. Figure 18 shows that Eq. (7) is in reasonable agreement with the full Mercier criterion for two equilibria, with (a) large aspect ratio A = 10, κ = 1.3, and (b) small aspect ratio A = 2.7, κ = 1.7. Figure 18 also shows the standard Shafranov–Yurchenko expression, which ignores the effect of ellipticity and fails to predict interchange instability at q = 1.

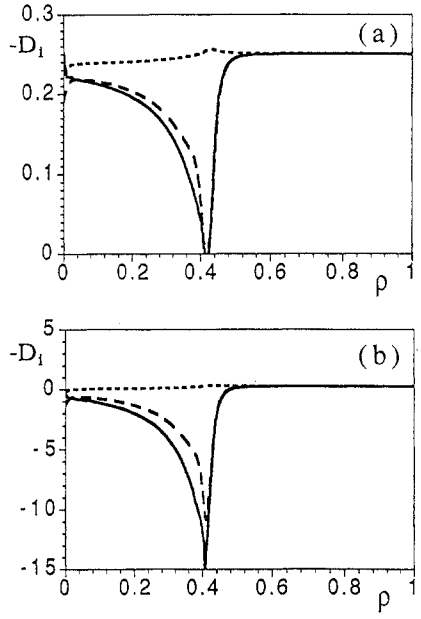

FIG. 18. Mercier criterion for an equilibrium with elliptic cross-section and low shear around the q = 1 surface. The solid line denotes the full criterion (Eq. (A.1)), the curve with long dashes denotes the large aspect ratio expansion with ellipticity (7), and the curve with short dashes denotes the Shafranov–Yurchenko approximation. (a) A = 10, κ = 1.3, and (b) A = 2.7, κ = 1.7.

An approximation of Eq. (7) that is often useful for the internal kink mode is obtained by considering almost flat current profiles with q' small and E/r and T/r^2 constant. Together with q = 1, this gives

$$-D_I \approx \frac{1}{4} + \frac{rp'}{s^2B^2}\frac{3E}{r}\left(1 - \frac{8T}{r}\frac{R_0}{r}\right) \quad (8)$$

Equation (8) shows that for sufficient ellipticity, ideal interchange instability can occur for modest pressure and not so low shear. As an example, we assume that the pressure profile is parabolic, which gives $\beta_p = -(p'/rB^2)(R_0^2q^2/2)$, and that triangularity is negligible. The Mercier criterion (8) then reduces to $\beta_p < s^2/(24e\epsilon^2)$. Even though the expansion to first order in ellipticity is not very accurate for JET geometry, we consider a JET-like case with $\epsilon_{q=1} = 0.16$ and $e_{q=1} = 0.2$, for which Eq. (8) gives $\beta_p < 8\,s^2$. This criterion is violated for rather modest pressures when the shear is less than about 0.1. For low shear, say $s \leq 0.03$, even a minute pressure gradient will violate the Mercier criterion at q = 1 in an elongated tokamak.

[1] After completion of this work, we learned that a similar expansion has been carried out by Fitzpatrick et al. [15]. They obtained an expression for the Mercier criterion that is different from our Eq. (7). The differences have been discussed by the authors and resolved in favour of the present Eq. (7).

4. SUMMARY

For circular cross-sections, the ideal MHD stability of the internal kink is relatively uncomplicated and is quite well described by large aspect ratio theory. We have modified the large aspect ratio calculation of Bussac et al. [1] with respect to the boundary conditions so that it applies for tokamak equilibria with $q_a > 2$. With this modification, the large aspect ratio expansion typically predicts β_p limits in the range of 0.1 to 0.2, in good agreement with our full MHD results. Most current profiles give β_p limits that decrease monotonically with increasing $q = 1$ radius. Both large aspect ratio theory and numerical computations show instability at low values of q_0. The stability of the internal kink is dependent on the current profile; for example, the Shafranov profile is less stable than profiles that are rounded in the central region, while current profiles with shoulders just outside the $q = 1$ surface are more stable.

With regard to shaping, we have found that ellipticity can significantly reduce the β_p limit. For JET geometry, typical values of the marginal β_p are between 0.03 and 0.1. The reduction of the pressure limit by elongation is accentuated in cases of weak shear in the $q \leq 1$ region, correlated with violation
of the Mercier criterion. Equation (7) gives the large aspect ratio form of the Mercier criterion including the lowest order effects of ellipticity and triangularity.

Finally, we remark that the internal kink mode is a weak MHD instability which can be strongly modified by a multitude of other effects such as resistivity, trapped particles, diamagnetic rotation and electron inertia. Such corrections can be expected to be particularly important when the shear at $q = 1$ is weak and the stability is sensitive to various small effects. In addition, the non-linear behaviour may deviate from the indications of linear theory. Nevertheless, it is important to know the result of linear, ideal MHD with some precision in order to be able to develop more sophisticated models with confidence.

Appendix

EXPANSION FOR THE MERCIER CRITERION

The Mercier criterion in axisymmetric geometry is given [8, 13, 14] by

$$-D_I \equiv \left(\frac{p' G I_2}{q'} - \frac{1}{2}\right)^2 + \frac{p'}{q'^2}\,(I_5' - p' I_3)\,(G^2 I_1 + I_4) > 0 \qquad (A.1)$$

Here, the equilibrium field is represented as $\vec{B} = \nabla\phi \times \nabla\psi + G(\psi)\,\nabla\phi$, the flux surface integrals are defined as

$$\{I_1, I_2, I_3, I_4, I_5\} = \int_{\psi = \text{const}} \frac{J\,d\omega}{2\pi} \times \left\{\frac{1}{R^2|\nabla\psi|^2}, \frac{1}{|\nabla\psi|^2}, \frac{R^2}{|\nabla\psi|^2}, \frac{1}{R^2}, 1\right\} \qquad (A.2)$$

and J is the Jacobian from (ψ, ω, ϕ) to Cartesian co-ordinates.

We introduce the (r, ω) co-ordinates as in Eq. (6) and consider the limit $\epsilon \to 0$ with β_p finite. Thus, we write $G = R_0 B_0 g(r)$, with $g = 1 + O(\epsilon^2)$, $p/B_0^2 = O(\epsilon^2)$ and $d\psi/dr = R_0 B_0 \epsilon f(r)$. The first step of the calculation is to express the metric tensor $g_{rr} = |\partial\vec{r}/\partial r|^2$, $g_{r\omega} = (\partial\vec{r}/\partial r)\cdot(\partial\vec{r}/\partial\omega)$, $g_{\omega\omega} = |\partial\vec{r}/\partial\omega|^2$ and the Jacobian $J = R\,\partial(R, Z)/\partial(r, \omega)$ as functions of r and ω by differentiating Eq. (6). Next, we need equilibrium relations from the Grad–Shafranov equation, which, in (r,ω) co-ordinates, reads

$$\frac{f}{J}\left[\frac{\partial}{\partial r}\left(\frac{f g_{\omega\omega}}{J}\right) - \frac{\partial}{\partial\omega}\left(\frac{f g_{r\omega}}{J}\right)\right] + \frac{p'}{R_0^2 B_0^2} + \frac{g g'}{R^2} = 0 \qquad (A.3)$$

where the prime denotes $\epsilon^{-1} d/dr$. The Grad–Shafranov equation is then expanded in ϵ and e. The ω independent piece gives the cylindrical pressure balance equation

$$g' + p'/B_0^2 + (f/r)\,(rf)' = 0 \qquad (A.4)$$

that allows us to eliminate g'. Equations for the Shafranov shift and the elliptic and the triangular deformation of the flux surfaces are obtained from the $\cos\omega$ component at $O(\epsilon)$, the $\cos 2\omega$ component at O(e) and the $\cos 3\omega$ component at $O(\epsilon)$, respectively:

$$\Delta'' + \left(\frac{2f'}{f} + \frac{1}{r}\right)\Delta' = \frac{1}{R_0} - \frac{2rp'}{R_0 B_0^2 f^2} + e\left[E\left(\frac{3p'}{R_0 B_0^2 f^2} - \frac{3\Delta'}{r^2} + \frac{12T}{r^3} + \frac{5T'}{r^2} + \frac{2Tf'}{r^2 f}\right) + E'\left(\frac{3rp'}{R_0 B_0^2 f^2} + \frac{3\Delta' f'}{f} + \frac{10T}{r^2} + \frac{2T'}{r} - \frac{3T'f'}{f} - \frac{1}{R_0}\right)\right] \qquad (A.5)$$

$$E'' + \left(\frac{2f'}{f} + \frac{1}{r}\right)E' - \frac{3}{r^2}E = 0 \qquad (A.6)$$

$$T'' + \left(\frac{2f'}{f} + \frac{1}{r}\right) T' - \frac{8}{r^2} T$$

$$= e\left[E\left(\frac{p'}{R_0 B_0^2 f^2} + \frac{3\Delta'}{r^2}\right)\right.$$

$$\left. - E'\left(\frac{3rp'}{R_0 B_0^2 f^2} + \frac{4\Delta'}{r} + \frac{3\Delta' f'}{f} - \frac{1}{R_0}\right)\right] \quad (A.7)$$

Of course, Eqs (A.4) to (A.7) contain higher order corrections, which do not contribute to the Mercier criterion at the order considered here. For the geometric coefficients, it is convenient to choose the ϵ^3 terms in Eq. (6) (represented by P, although, in fact, there are more terms at this order) such that $\int (J/R^2) d\omega = 2\pi r/R_0$. This amounts to defining a free normalization constant at higher order in ϵ. With this choice, f can be expressed in terms of the safety factor: $f = rg/qR_0$. To perform the flux surface integrals, we also need $|\nabla r|^2 = g^{rr} = R^2 g_{\omega\omega}/J^2$. To the required order, we obtain

$$I_1 = \frac{R_0^2 q^3}{r^2 G^3}\left[1 + c_0 - 3c_2 - \epsilon^2\left(\frac{r^2}{R_0^2} + \frac{2\Delta}{R_0}\right)\right.$$

$$\left. + e\epsilon^2 E \frac{3r}{2R_0^2}\right] \quad (A.8a)$$

$$I_2 = \frac{R_0^4 q^3}{r^2 G^3}\left[1 + c_0 + 3c_1 + 3c_2 - \epsilon^2\right.$$

$$\left. \times \left(\frac{3r^2}{2R_0^2} + \frac{4\Delta + 3r\Delta'}{R_0}\right) + e\epsilon^2 \frac{9rE + 3r^2E'}{4R_0^2}\right] \quad (A.8b)$$

$$I_3 = \frac{R_0^6 q^3}{r^2 G^3}\left[1 + c_0 + 6c_1 + 9c_2 - \epsilon^2 \frac{6\Delta + 6r\Delta'}{R_0}\right.$$

$$\left. - e\epsilon^2 \frac{3r^2 E'}{2R_0^2}\right] \quad (A.8c)$$

$$I_4 = \frac{q}{G} \quad (A.8d)$$

$$I_5 = \frac{R_0^2 q}{G}\left[1 + c_1 - \epsilon^2\left(\frac{r^2}{2R_0^2} + \frac{2\Delta}{R_0} + \frac{r\Delta'}{R_0}\right)\right.$$

$$\left. + e\epsilon^2 \frac{3rE + r^2E'}{4R_0^2}\right] \quad (A.8e)$$

where c_0 contains the $O(\epsilon^3)$ shaping corrections in Eq. (6) and

$$c_1 = e\epsilon^2 \frac{(rET)'}{rR_0} \quad (A.9a)$$

$$c_2 = e\epsilon^2 E' \frac{r(\Delta' - T')}{2R_0} \quad (A.9b)$$

Substituting Eqs (A.8) into Eq. (A.1), we obtain expression (7) for the Mercier criterion.

ACKNOWLEDGEMENT

This work was funded in part by the Swiss National Science Foundation.

REFERENCES

[1] BUSSAC, M.N., PELLAT, R., EDERY, D., SOULÉ, J.L., Phys. Rev. Lett. **35** (1975) 1638.
[2] de BLANK, H.J., SCHEP, T.J., Phys. Fluids B **3** (1991) 1136.
[3] BONDESON, A., BUSSAC, M.-N., Nucl. Fusion **32** (1992) 513.
[4] TURNBULL, A.D., TROYON, F., Nucl. Fusion **29** (1989) 1887.
[5] CONNOR, J.W., HASTIE, R.J., The Effect of Shaped Plasma Cross Sections on the Ideal Internal Kink Mode in a Tokamak, Rep. CLM-M-106, Culham Laboratory, Abingdon, Oxfordshire (1985).
[6] BERGER, D., BERNARD, L.C., GRUBER, R., TROYON, F., in Plasma Physics and Controlled Nuclear Fusion Research 1976 (Proc. 6th Int. Conf. Berchtesgaden, 1976), Vol. 2, IAEA, Vienna (1977) 411.
[7] COPPI, A.C., COPPI, B., Nucl. Fusion **32** (1992) 205.
[8] BONDESON, A., VLAD, G., LÜTJENS, H., Phys. Fluids B **4** (1992) 1889.
[9] LÜTJENS, H., BONDESON, A., ROY, A., Comput. Phys. Commun. **69** (1992) 287.
[10] SOLTWISCH, H., STODIEK, W., MANICKAM, J., SCHLÜTER, J., in Plasma Physics and Controlled Nuclear Fusion Research 1986 (Proc. 11th Int. Conf. Kyoto, 1986), Vol. 1, IAEA, Vienna (1987) 263.
[11] HOLMES, J.A., CARRERAS, B.A., CHARLTON, L.A., Phys. Fluids B **1** (1989) 788.
[12] EDERY, D., LAVAL, G., PELLAT, R., SOULÉ, J.L., Phys. Fluids **19** (1976) 260.
[13] GLASSER, A.H., GREENE, J.M., JOHNSON, J.L., Phys. Fluids **18** (1975) 875; KUVSHINOV, B.N., Sov. J. Plasma Phys. **17** (1991) 79; Fiz. Plazmy **17** (1991) 139.

[14] FREIDBERG, J.P., in Ideal Magnetohydrodynamics, Plenum Press, New York (1987) Ch. 10; LAVAL, G., LUC, H., MASCHKE, E.K., MERCIER, C., PELLAT, R., in Plasma Physics and Controlled Nuclear Fusion Research 1971 (Proc. 4th Int. Conf. Madison, 1971), Vol. 2, IAEA, Vienna (1971) 507; LORTZ, D., NÜHRENBERG, J., Nucl. Fusion **13** (1973) 821.

[15] FITZPATRICK, R., GIMBLETT, C.G., HASTIE, R.J., Plasma Phys. Control. Fusion **34** (1992) 161.

[16] SHAFRANOV, V.D., YURCHENKO, E.I., Sov. Phys. — JETP **26** (1968) 682.

[17] GLASSER, A.H., GREENE, J.M., JOHNSON, J.L., Phys. Fluids **19** (1976) 567.

(Manuscript received 6 April 1992
Final manuscript received 15 July 1992)